Effective long-range interlayer interactions and electric-field-induced subphases in ferrielectric liquid crystals

A. D. L. Chandani,[1,2] Atsuo Fukuda,[1,*] Jagdish K. Vij,[1,†] Yoichi Takanishi,[3] and Atsuo Iida[4]

[1]*Department of Electronic and Electrical Engineering, Trinity College, The University of Dublin, Dublin 2, Ireland*

[2]*Department of Chemistry, University of Peradeniya, Peradeniya, Sri Lanka*

[3]*Department of Physics, Kyoto University, Kyoto 606-8502, Japan*

[4]*Photon Factory, Institute of Materials Structure Science, High Energy Accelerator Research Organization, Ibaraki 305-0801, Japan*

(Received 30 October 2015; revised manuscript received 27 January 2016; published 19 April 2016)

Microbeam resonant x-ray scattering experiments recently revealed the sequential emergence of electric-field-induced subphases (stable states) with exceptionally large unit cells consisting of 12 and 15 smectic layers. We explain the emergence of the field-induced subphases by the quasimolecular model based on the Emelyanenko-Osipov long-range interlayer interactions (LRILIs) together with our primitive way of understanding the frustration in clinicity using the q_E number defined as $q_E = |[R] - [L]|/([R] + [L])$; here $[R]$ and $[L]$ refer to the numbers of smectic layers with directors tilted to the right and to the left, respectively, in the unit cell of a field-induced subphase. We show that the model actually stabilizes the field-induced subphases with characteristic composite unit cells consisting of several blocks, each of which is originally a ferrielectric three-layer unit cell stabilized by the LRILIs, but some of which would be modified to become ferroelectric by an applied electric field. In a similar line of thought, we also try to understand the puzzling electric-field-induced birefringence data in terms of the LRILIs.

DOI: 10.1103/PhysRevE.93.042707

I. INTRODUCTION

A series of experimental studies [1–4] has revealed the sequential emergence of temperature-induced biaxial and uniaxial subphases as a result of degeneracy lifting due to long-range interlayer interactions (LRILIs) at the frustration points among antiferroelectric smectic-C_A^* (Sm-C_A^*), ferroelectric Sm-C^*, and paraelectric Sm-A phases [5–10]. The biaxial subphases have nonplanar superlattice structures with highly distorted microscopic short-pitch helical director arrangements in unit cells consisting of several smectic layers [11–23]. Since the deviation from the planar structures is not really large, however, the biaxial subphases are appropriately specified by a relative ratio of ferroelectric and antiferroelectric orderings in the unit cell

$$q_T = \frac{[F]}{[A] + [F]}. \tag{1}$$

Here q_T typically increases monotonically from 0 in the antiferroelectric Sm-C_A^* phase to 1 in the ferroelectric Sm-C^* phase with rising temperature, as the degeneracy lifting is frequently due to weak LRILIs at the frustration point between the main phases Sm-C_A^* and Sm-C^* [1–4]. Subphases with smaller unit cells of irreducible q_T in lower terms in the denominator must be observed more easily, whereas those with larger unit cells of irreducible q_T in higher terms in both the numerator and denominator may be suppressed by a number of factors including surface and finite-size effects and thermal fluctuations. Experimentally, seven subphases with $q_T = 1/5$, $1/4$, $1/3$, $2/5$, $1/2$, $3/5$, and $2/3$ are considered to exist [1–4,23–27].

In this paper we study the electric-field-induced subphases (stable states) and their emerging sequences along a similar line of thought. Increasing applied electric field produces nearly the same effects as increasing temperature; both favor the ferroelectric state. Since an applied electric field selectively determines the director tilting sense, we should use

$$q_E = \frac{|[R] - [L]|}{[R] + [L]} \tag{2}$$

instead of q_T; here $[R]$ and $[L]$ refer to the numbers of smectic layers with directors tilted to the right and to the left, respectively, in the unit cell of a field-induced subphase.[1] Sequential characteristics of the field-induced transitions have been observed in several temperature-induced subphase regions at zero electric field, $q_T = 1/4$, $1/3$, $1/2$, $3/5$, and $2/3$, from the early stage of investigation [1–4,27–32]. All of the antiferroelectric phases, $q_T = 0$ (Sm-C_A^*), $1/4$, $1/2$, and $2/3$, must have $q_E = 0$ at zero electric field, whereas ferrielectric and ferroelectric phases, $q_T = 1/3$, $3/5$, $2/3$, and 1 (Sm-C^*), must have $q_E = 1/3$, $1/5$, $1/3$, and 1, respectively. The LRILIs are usually weak and hence q_E may increase monotonically with increasing applied electric field.

Sandhya *et al.* recently found a fairly conspicuous example of the field-induced transition from $q_E = 1/5$ ($q_T = 3/5$) to $q_E = 3/5$, which is considered to occur by flipping only one layer in the five-layer unit cell of the temperature-induced subphase with $q_T = 3/5$ [27]. Sandhya *et al.* also observed at least two, probably three field-induced subphases in the transition from $q_E = 1/3$ ($q_T = 1/3$) to $q_E = 1$ (Sm-C^*)

*fukudaa@tcd.ie

†jvij@tcd.ie

[1]When q_E was introduced at the early stage of investigation [2], it was defined as $q_E = [R]/([R] + [L])$. Since this definition is asymmetric with respect to R and L, however, it would be better to define symmetrically as given above.

[4,32]. Prior to these observations having been reported, the general view seemed to have been that on applying the field $q_E = 1/3$ ($q_T = 1/3$) went directly to $q_E = 1$. Conceivable simple q_E's in this case are 1/3, 1/2, 3/5, 2/3, etc., although it may directly change into the unwound Sm-C^* phase by simultaneously flipping one layer in the simple three-layer unit cell of the temperature-induced subphase with $q_T = 1/3$. Actually, however, Sandhya *et al.* pointed out some sequential characteristics of the field-induced subphase emergence that may indicate the stable existence of at least two subphases before the field-induced transition into the unwound Sm-C^* phase. We were wondering at that stage of our work what unit cells constituted these field-induced subphases.

Microbeam resonant x-ray scattering (RXRS) experiments brought about a breakthrough in confirming the emergence of the field-induced subphases that have unbelievably large 12- and 15-layer unit cells [33]. Moreover, they clarified the approximate planar superlattice structure of the 12-layer unit cell with $q_E = 2/3$: It consists of four blocks, each of which is originally ferrielectric 3-layer unit cells stabilized by the LRILIs, but with two consecutive blocks that would be modified to become ferroelectric by an applied electric field. There are several theoretical approaches to describe the sequential phase transitions in polar smectic liquid crystals, but only two of them have presented definite results that can be compared with the experimental ones. One is the phenomenological Landau model reported by Dolganov *et al.* [34,35] and the other is the partially molecular model based on the LRILIs proposed by Emelyanenko and Osipov [36,37]. Apparently, the Landau model looks simple and straightforward, but actually it is a mathematically complicated task to perform minimization over the set of two-component order parameters. In the partially molecular model, on the other hand, such a difficulty does not exist and the LRILIs are simple, natural, and effective in explaining the sequential emergence of temperature-induced biaxial subphases. Therefore, our objective is to examine whether the quasimolecular model can explain the emergence of such unexpected exceptional field-induced subphases with unit cells containing as many as 12 and 15 smectic layers. In the following, we will show that the model actually stabilizes the field-induced subphases with characteristic composite unit cells consisting of several blocks, each of which is originally ferrielectric three-layer unit cells stabilized by the LRILIs, but some of which would be modified to become ferroelectric by an applied electric field.

II. FREE ENERGY OF FIELD-INDUCED SUPERLATTICE STRUCTURES ANALYZED BY THE QUASIMOLECULAR MODEL

The LRILIs proposed by Emelyanenko and Osipov [36,37] are useful for understanding the degeneracy lifting at the frustration point, when the tilt angle can be considered approximately constant and the two prototypal subphases with $q_T = 1/3$ and $1/2$ emerge between the Sm-C_A^* and Sm-C^* phases. They numerically calculated the subphase unit-cell structures and the stability ranges by using the free energy

$$F = \sum_{i=1}^{N} (F_i + \Delta F_i), \tag{3}$$

where N is the total number of smectic layers. The polarization-independent part F_i is phenomenologically given by

$$F_i = F_0(\theta) - \frac{\alpha(T - T^*)}{T^*}(\cos\phi_{i-1,i} + \cos\phi_{i,i+1}) - b(\cos^2\phi_{i-1,i} + \cos^2\phi_{i,i+1}), \tag{4}$$

where $\alpha > 0$ and $b > 0$ are constants and T^* is the transition temperature between the anticlinic antiferroelectric Sm-C_A^* and synclinic ferroelectric Sm-C^* phases, which are stabilized for $T < T^*$ and $T > T^*$, respectively.

The polarization-dependent part ΔF_i is written as

$$\Delta F_i = \frac{1}{2\chi}\left\{\mathbf{P}_i^2 + g(\mathbf{P}_{i-1}\cdot\mathbf{P}_i + \mathbf{P}_i\cdot\mathbf{P}_{i+1})\right\} + c_{\mathrm{p}}(\mathbf{P}_i\cdot\boldsymbol{\xi}_i) + c_{\mathrm{f}}\cos\theta\{\mathbf{P}_i\cdot(\mathbf{n}_{i+1} - \mathbf{n}_{i-1})\}, \tag{5}$$

which consists of the last two terms containing the piezoelectric and flexoelectric coefficients c_{p} and c_{f}, respectively, and the first term of the polarization-polarization interactions. Here g represents the molecular positional correlation in adjacent layers and $\boldsymbol{\xi}_i$ is given by

$$\boldsymbol{\xi}_i \equiv \cos\theta[\mathbf{n}_i \times \mathbf{e}]. \tag{6}$$

The tilt angle θ is assumed to be independent of temperature and spatially uniform and $\mathbf{n}_i$ and $\mathbf{e}$ are the director and the smectic layer normal, respectively. They reasonably take account of the direct couplings between adjacent layers only; it is hard to consider any direct coupling between smectic layers separated in next-nearest-neighbor positions or beyond, since smectics have no long-range positional order.

The effect of an applied electric field $\mathbf{E}$ can be taken into account by adding a term $\mathbf{P}_i\cdot\mathbf{E}$ in Eq. (5). This way of including the electric-field effect has been widely used in several papers [38–47]. The three papers by Emelyanenko [45–47] are elaborate and extended versions of his prototypal paper with Osipov [36]. In these papers, the way of minimizing the free energy is characteristic and the tensorial nature of g is also taken into account. The apparently main conclusion illustrated in Figs. 1 and 2 of Ref. [45] is, however, in contradiction with the established view that the tilting directions are parallel to the field in the unwound antiferroelectric phase [2,39]. Moreover, the structure of a 15-layer subphase obtained as $q_T = 11/15$ in his most recent paper [47] is different from that identified in this paper. In the following, therefore, we try to understand the emergence of field-induced subphases with exceptionally large unit cells consisting of 12 and 15 smectic layers by using the simple quasimolecular model and the electric field effect $\mathbf{P}_i\cdot\mathbf{E}$.

Minimizing the total free energy including the field effect with respect to polarization $\mathbf{P}_i$ results in effective LRILIs. Actually, by performing the minimization, we obtain the following set of equations for $\mathbf{P}_i$:

$$\mathbf{P}_i + g(\mathbf{P}_{i-1} + \mathbf{P}_{i+1}) + \chi\mathbf{M}_i^E = 0, \tag{7}$$

where

$$\mathbf{M}_i^E \equiv \mathbf{M}_i + \mathbf{E} \tag{8}$$

and

$$\mathbf{M}_i \equiv c_{\mathrm{p}}\boldsymbol{\xi}_i + c_{\mathrm{f}}\cos\theta(\mathbf{n}_{i+1} - \mathbf{n}_{i-1}). \tag{9}$$

Now the polarization-dependent part of the free energy including the applied electric-field effect is written as follows:

$$\Delta F_i = \tfrac{1}{2}\mathbf{P}_i \cdot \mathbf{M}_i^E. \tag{10}$$

Analytical solutions for Eq. (7) can be obtained for any field-induced superlattice structures with unit cells consisting of a finite number of smectic layers. For a unit cell consisting of any odd number of layers $t = 2n + 1$, we obtain

$$\mathbf{P}_i^{(2n+1)} = -\frac{\chi}{r_{2n+1}}\left[s_{2n+1}\mathbf{M}_i^{(E)} + \sum_{k=1}^{n}(-g)^k s_{2(n-k)+1}\left(\mathbf{M}_{i-k}^{(E)} + \mathbf{M}_{i+k}^{(E)}\right)\right]. \tag{11}$$

For a unit cell consisting of any even number of layers $t = 2n$, on the other hand, we obtain

$$\mathbf{P}_i^{(2n)} = -\frac{\chi}{r_{2n}}\left[s_{2n}\mathbf{M}_i^{(E)} + \sum_{k=1}^{n-1}(-g)^k s_{2(n-k)}\left(\mathbf{M}_{i-k}^{(E)} + \mathbf{M}_{i+k}^{(E)}\right)\right] + \frac{1}{2}(-g)^n s_0\left(\mathbf{M}_{i-n}^{(E)} + \mathbf{M}_{i+n}^{(E)}\right). \tag{12}$$

The coefficients r_k and s_k are given in Eqs. (55), (56), (58), and (59) of Ref. [36].

Substituting Eqs. (11) and (12) into Eq. (10), we obtain the following expression for the polarization contribution to the free energy of the superlattice structure with a periodicity of t layers:

$$\frac{\Delta F_t}{N} = -\frac{\chi}{2t}\sum_{i=1}^{t}\sum_{k=1}^{t} f_k \mathbf{M}_i^{(E)} \cdot \mathbf{M}_{i+k-1}^{(E)}, \tag{13}$$

where f_k is given in Eq. (61) of Ref. [36]. Substituting Eq. (8) into Eq. (13), we obtain

$$\frac{\Delta F_t}{N} = -\frac{\chi}{2t}\sum_{i=1}^{t}\sum_{k=1}^{t} f_k \mathbf{M}_i \cdot \mathbf{M}_{i+k-1} - \frac{\chi E^2}{2(1+2g)} - \frac{\chi c_{\mathrm{p}} E \sin\theta\cos\theta}{(1+2g)t}\sum_{i=1}^{t}\cos\varphi_i, \tag{14}$$

where the director is expressed in terms of the tilt angle θ and the azimuthal angle φ_i,

$$\mathbf{n}_i = (\sin\theta\cos\varphi_i, \sin\theta\sin\varphi_i, \cos\theta), \tag{15}$$

and the electric field is applied along the y axis,

$$\mathbf{E} = (0, E, 0). \tag{16}$$

Since the first term of Eq. (14) is given in Eq. (62) of Ref. [36], we obtain the modified dimensionless free-energy density of any t-layer field-induced superlattice structure $\tilde{F}_t$, which can be used to find the most stable one at a particular temperature and an applied electric field:

$$\begin{aligned}\tilde{F}_t &= \frac{1}{B\sin^2(\theta)\cos^2(\theta)}\left\{\frac{F_t}{N} - F_0(\theta) + \frac{\chi E^2}{2(1+2g)}\right\} \\ &= -\frac{1}{2}\frac{\chi c_{\mathrm{p}} c_{\mathrm{f}}}{B}\left\{\frac{c_{\mathrm{p}}}{c_{\mathrm{f}}} f_1 + \frac{c_{\mathrm{f}}}{c_{\mathrm{p}}} f_1^{(2)}\right\} \\ &\quad - \frac{\chi c_{\mathrm{p}} c_{\mathrm{f}}}{B}\frac{1}{t}\sum_{i=1}^{t-1}\sum_{j=i+1}^{t}\left\{\frac{c_{\mathrm{p}}}{c_{\mathrm{f}}} f_{j-i+1} + \frac{c_{\mathrm{f}}}{c_{\mathrm{p}}} f_{j-i+1}^{(2)}\right\}\cos(\varphi_j - \varphi_i) \\ &\quad + 2\frac{\chi c_{\mathrm{p}} c_{\mathrm{f}}}{B}\frac{1}{t}\sum_{i=1}^{t-1}\sum_{j=i+1}^{t} f_{j-i+1}^{(1)}\sin(\varphi_j - \varphi_i) \\ &\quad - \frac{1}{t}\sum_{i=1}^{t}\cos^2(\varphi_{i+1} - \varphi_i) - \frac{a\Delta T}{BT^*}\frac{1}{t}\sum_{i=1}^{t}\cos(\varphi_{i+1} - \varphi_i) \\ &\quad - \frac{\chi c_{\mathrm{p}} E}{\sin\theta\cos\theta B(1+2g)}\frac{1}{t}\sum_{i=1}^{t}\cos\varphi_i,\end{aligned} \tag{17}$$

where $a = 2\alpha/(\sin^2\theta\cos^2\theta)$ and $B = 2b/(\sin^2\theta\cos^2\theta)$. Five parameters are needed, four of which have already been used in Ref. [36] and are intuitively understandable: g (the molecular positional correlation in adjacent layers), $c_{\mathrm{f}}/c_{\mathrm{p}}$ (the ratio between flexoelectric and piezoelectric coefficients), $\chi c_{\mathrm{p}} c_{\mathrm{f}}/B$ (the strength of LRILIs as compared to that of short-range interlayer interactions), and $\tilde{T} = a\Delta T/BT^*$ (the effective dimensionless temperature); the only new parameter is the effective dimensionless electric-field strength

$$\tilde{E} = \chi c_{\mathrm{p}} E/\{\sin\theta\cos\theta B(1+2g)\}. \tag{18}$$

When $\tilde{E} = 0$, the free energy $\tilde{F}_t$ ensures that all the subphases are antisymmetrical with respect to their middles of their unit cells and is minimized with respect to $\varphi_{i,j} \equiv \varphi_j - \varphi_i$ as given in Eq. (65) of Ref. [36]. Since the electric field generally changes the symmetry of field-induced subphases, minimizing Eq. (17) with respect to φ_i is not as easy as it would appear to be. In order to see how to properly perform the minimization, therefore, let us first consider some simple cases of the main phases and the subphases.

III. CASE-BY-CASE STUDIES OF THE ELECTRIC-FIELD EFFECTS IN SOME SIMPLE UNIT-CELL STRUCTURES

Two major effects produced in a main phase or subphase by applying an electric field are unwinding of the macroscopic long-pitch helical structure and aligning of the averaged tilt-plane direction of the unit cell with respect to the electric field. Since no macroscopic long-pitch helical structure is taken into account in Eq. (17), the aligning starts to occur from the beginning $\tilde{E} \simeq 0$. Let us begin with the two simple structures of the main phases, the ferroelectric Sm-C^* and antiferroelectric Sm-C_A^* phases, where the directors of the whole smectic layers are parallel to a single plane and hence the structure is planar. The free energy given by Eq. (17) is written for the Sm-C^* phase as

$$\tilde{F}_1 = -1 - \tilde{T} - \frac{1}{2(1+2g)}\frac{c_{\mathrm{p}}}{c_{\mathrm{f}}}\frac{\chi c_{\mathrm{p}} c_{\mathrm{f}}}{B} - \tilde{E}\cos\varphi_1 \tag{19}$$

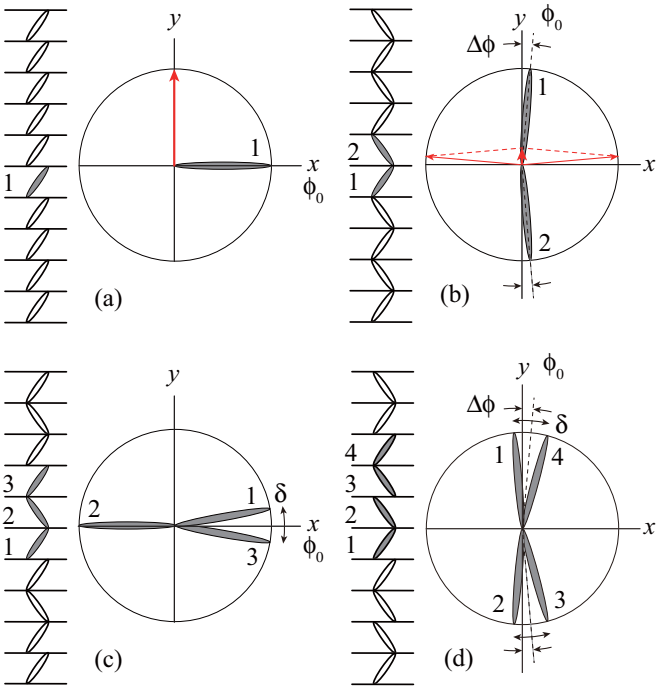

FIG. 1. Electric-field effects in (a) Sm-C^*, (b) Sm-C^*_A, (c) $q_T = 1/3$, and (d) $q_T = 1/2$. The averaged tilt plane direction is perpendicular to the applied electric field in the (a) ferroelectric and (c) ferrielectric phases. It may become parallel to the electric field in the (b) and (d) antiferroelectric phases; at the same time, the directors in the unit cell may show some small asymmetric change to produce induced polarization in the initial averaged tilt direction, which is observed as the pretransitional effect in the antiferroelectric phases [38–40,48–50]. The electric field is applied along the y direction.

and hence we have $\cos\varphi_1 = 1$, i.e., $\varphi_1 = 0$, for $\tilde{E} > 0$. Since $\tilde{E}$ contains the product of $c_p E$ as in Eq. (18), $\tilde{E} > 0$ means $c_p > 0$ for an electric field applied along the y axis; the director tilting occurs parallel to the x axis in the $\varphi_1 = 0$ direction as intuitively anticipated from Eqs. (9) and (11) and illustrated in Fig. 1(a). In other words, $c_p > 0$ corresponds to the positive spontaneous polarization.

In the main antiferroelectric phase Sm-C^*_A, it is well known that the director tilting plane tends to be parallel to the electric field and some small nonplanar (asymmetric) distortion occurs in the planar anticlinic structure as the pretransitional effect [38–40,48–50]. Let us consider that the initial tilt-plane direction is ϕ_0 and the distortion angle is $\Delta\phi$. Then we can set

$$\varphi_1 = \phi_0 - \Delta\phi, \quad \varphi_2 = \phi_0 + \pi + \Delta\phi. \tag{20}$$

We determine their equilibrium values by minimizing Eq. (17) with respect to ϕ_0 and $\Delta\phi$ as follows:

$$\begin{aligned} \phi_0 &= \pm\frac{\pi}{2}, \\ \Delta\phi &= \pm\frac{\tilde{E}}{4\{2 - \tilde{T} + g(c_p/c_f)(\chi c_p c_f/B)/(1-4g^2)\}}. \end{aligned} \tag{21}$$

As illustrated in Fig. 1(b), in fact, such a distortion produces a small induced spontaneous polarization along the initial tilt-plane direction $\phi_0 = \pm\pi/2$; the resulting polarization makes the initial tilt-plane direction align along the applied electric field. Again, $c_p > 0$ corresponds to the positive spontaneous polarization consistently.

The structures of all temperature-induced subphases produced by the Emelyanenko-Osipov LRILIs are not planar and possess a certain symmetry that is visible when the structures are viewed along the smectic layer normal. In fact, the tilt directions in different layers are antisymmetric with respect to the middle of the period. This property defines the chirality of the short-pitch deformed helix structures of these subphases as well as a characteristic plane with respect to which the director tilting directions of all smectic layers are arranged symmetrically [36]. In the three-layer field-induced superlattice structure in the temperature region of Sm-C^*_A ($q_T = 1/3$), we can check numerically, using Eq. (17) on the assumption of a small deviation from the Ising structure, that the unit cell actually aligns as illustrated in Fig. 1(c). It is also intuitively clear that the averaged tilt-plane direction is arranged perpendicular to the applied electric field.

In this way we can set

$$\varphi_1 = \phi_0 + \frac{\delta}{2}, \quad \varphi_2 = \phi_0 + \pi, \quad \varphi_3 = \phi_0 - \frac{\delta}{2} \tag{22}$$

and obtain the free energy given in Eq. (17) as a function of ϕ_0 and δ. By minimizing the free energy with respect to ϕ_0 and δ, in fact, we determine these variables as follows:

$$\begin{aligned} \phi_0 &= 0, \\ \delta &= -\frac{8(1+2g)(\chi c_p c_f/B)}{(1+g-2g^2)(6+\tilde{T}+\tilde{E}) + (\chi c_p c_f/B)\{(1+2g)(c_f/c_p) + g(c_p/c_f)\}}. \end{aligned} \tag{23}$$

Since $\tilde{E}$ contains the product of $c_p E$ and the electric field is applied along the y axis, $\phi_0 = 0$ indicates that the averaged tilt-plane direction is perpendicular to the electric field and the unit cell has positive spontaneous polarization for $c_p > 0$. Since δ and $c_p c_f$ have opposite signs, the short-pitch deformed helix is right handed for $c_p c_f < 0$ and left handed for $c_p c_f > 0$.

In the four-layer superlattice structure of the antiferroelectric Sm-C^*_A phase ($q_T = 1/2$), there also exists an averaged tilt plane with respect to which the director tilting directions and senses of all smectic layers are arranged symmetrically. Contrary to the three-layer superlattice structure of the ferrielectric Sm-C^*_A phase ($q_T = 1/3$), however, both director tilting senses in the averaged tilt plane are equivalent; there is neither a favorable nor an unfavorable director tilting sense. It is well known that the averaged tilt plane becomes parallel to the electric field and at the same time, the directors in the unit cell show some small asymmetric movement indicating a pretransitional change from antiferroelectric to ferroelectric as shown in Fig. 1(d). It would

be convenient to set

$$\varphi_1 = \phi_0 - \Delta\phi + \frac{\delta}{2}, \quad \varphi_2 = \phi_0 + \pi + \Delta\phi - \frac{\delta}{2},$$
$$\varphi_3 = \phi_0 + \pi + \Delta\phi + \frac{\delta}{2}, \quad \varphi_4 = \phi_0 + 2\pi - \Delta\phi - \frac{\delta}{2}, \tag{24}$$

where ϕ_0 is the initial average tilt-plane direction at $\tilde{E} = 0$, $\Delta\phi$ the asymmetric deformation, and δ the distortion angle representing the nonplanar unit-cell structure. Inserting Eq. (24) into Eq. (17), we obtain the free energy as a function of ϕ_0, $\Delta\phi$, and δ. By minimizing the free energy with respect to these variables, we determine the equilibrium values of ϕ_0, $\Delta\phi$, and δ as follows:

$$\phi_0 = \pm\frac{\pi}{2},$$
$$\delta = -\frac{\chi c_{\rm p} c_{\rm f}}{B}, \tag{25}$$
$$\Delta\phi = \pm\frac{\tilde{E}}{2\{2 - \tilde{T} + 2(c_{\rm f}/c_{\rm p})(\chi c_{\rm p} c_{\rm f}/B) + g(c_{\rm p}/c_{\rm f})(\chi c_{\rm p} c_{\rm f}/B)/(1+2g)\}}.$$

As shown in Fig. 1(d), in fact, such a distortion produces small induced spontaneous polarization along the initial tilt-plane direction $\phi_0 = \pm\pi/2$; the resulting polarization makes the initial tilt-plane direction align along the applied electric field. Again, $c_{\rm p} > 0$ corresponds to the positive polarization and the short-pitch distorted helical structure is right handed for $c_{\rm f} < 0$ and left handed for $c_{\rm f} > 0$. Moreover, it is very characteristic that δ is uniquely determined only by the fourth parameter and does not depend on the temperature $\tilde{T}$ and the applied electric field $\tilde{E}$ as already pointed out in Ref. [36] when $\tilde{E} = 0$.

IV. SEQUENTIAL EMERGENCE OF FIELD-INDUCED SUBPHASES

A. Formulation

As illustrated in Fig. 1, electric-field effects in antiferroelectric superlattice structures are quite different from those in ferroelectric and ferrielectric superlattice structures. In the antiferroelectric case, the applied field may produce some asymmetric distortion in the director arrangements indicating a pretransitional change from antiferroelectric to ferrielectric or ferroelectric [38–40,48–50] and may cause the disappearance of the characteristic plane with respect to which the director tilting directions of all smectic layers were arranged symmetrically when no field was applied. In the ferrielectric case, on the other hand, there is no reason to assume the disappearance of the characteristic plane, although the applied field may destroy the property due to the Emelyanenko-Osipov LRILIs that the tilt directions in different layers are antisymmetrical with respect to the middle of the period; the applied field only interacts with the piezoelectric polarization but not with the flexoelectric polarization as is clear in Eqs. (17) and (18). It is not impertinent to consider that the director tilting directions of all smectic layers are arranged symmetrically with respect to the characteristic plane in all field-induced superlattice structures that emerge on the higher field side of the three-layer $q_E = 1/3$ subphase; they must be ferrielectric as q_E increases with the applied field. This characteristic plane can be chosen as the z-x plane and the positive sense of the x axis is favorable for the director tilting when the electric field is applied along the y axis and $c_{\rm p} > 0$. The unit cell aligns so that this symmetrical plane becomes perpendicular to the applied electric field.

The applied field effect in the free energy of Eq. (17) is written as

$$-\tilde{E}\frac{1}{t}\sum_{n=1}^{t}\cos\varphi_n = -\tilde{E}\frac{1}{t}\sum_{n=1}^{t}\cos(\varphi_1 + \varphi_{1,n})$$
$$= -\tilde{E}\frac{1}{t}\sum_{n=1}^{t}\cos\left(\varphi_1 + \sum_{k=1}^{n-1}\varphi_{k,k+1}\right). \tag{26}$$

Notice that the other terms are the same as given in Eq. (62) of Ref. [36] and are already written in terms of $\varphi_{i,i+1} \equiv \varphi_{i+1} - \varphi_i$, where $i = 1,2,3,\ldots,t-1$. There are four cases in choosing φ_1 on the basis of the presence of the characteristic plane.

(i) When the t-layer unit cell under consideration has a layer where the director tilting occurs parallel to the characteristic plane and toward the positive sense of the x axis, we can choose this layer and set $\varphi_1 = 0^\circ$.

(ii) Similarly, if the director tilting is toward the negative sense of the x axis, we can set $\varphi_1 = 180^\circ$.

(iii) When the t-layer unit cell has adjacent layers that are arranged symmetrically with respect to the characteristic plane and their averaged director tilting is along the positive sense of the x axis, we can set $\varphi_1 = -\varphi_{1,2}/2$.

(iv) Similarly, if the director tilting is along the negative sense, we can set $\varphi_1 = 180^\circ - \varphi_{1,2}/2$.

In this way, we can fix the orientation of the t-layer unit cell in the applied electric field.

Now we try to obtain $\varphi_{i,i+1}$'s ($i = 1,2,3,\ldots,t-1$) that minimize the free energy given in Eq. (17). Performing partial differentiation with respect to $\varphi_{i,i+1}$, we obtain the following

$t-1$ sets of equations:

$$
\begin{aligned}
&2\frac{\chi c_{\rm p}c_{\rm f}}{B}\sum_{n=1}^{i}\sum_{m=i+1}^{t} f^{(1)}_{m-n+1}\cos\varphi_{n,m}\\
&\quad+\frac{\chi c_{\rm p}c_{\rm f}}{B}\sum_{n=1}^{i}\sum_{m=i+1}^{t}\left\{\frac{c_{\rm p}}{c_{\rm f}}f_{m-n+1}+\frac{c_{\rm f}}{c_{\rm p}}f^{(2)}_{m-n+1}\right\}\sin\varphi_{n,m}\\
&\quad+\sin(2\varphi_{i,i+1})+\sin\left(2\sum_{n=1}^{t-1}\varphi_{n,n+1}\right)\\
&\quad+\tilde{T}\left\{\sin\varphi_{i,i+1}+\sin\left(\sum_{n=1}^{t-1}\varphi_{n,n+1}\right)\right\}\\
&\quad+\tilde{E}\left\{-S\frac{\delta_{i,1}}{2}\sin\frac{\varphi_{1,2}}{2}+\sum_{n=i+1}^{t}\left(1-S\frac{\delta_{i,1}}{2}\right)\right.\\
&\quad\left.\times\sin\left(-S\frac{\varphi_{1,2}}{2}+\varphi_{1,n}\right)\right\}=0. \qquad (27)
\end{aligned}
$$

The first four terms on the left-hand side that do not depend on the applied field have already been obtained in Eq. (65) of Ref. [36]. The last term represents the electric-field effect, where S is

$$
S=\begin{cases}0 & \text{for cases (i) and (ii)}\\ 1 & \text{for cases (iii) and (iv).}\end{cases} \qquad (28)
$$

Field-induced subphases may be nonplanar, but the actual structure does not deviate largely from the corresponding planar prototype. The angles $\varphi_{n,m}$ may be split into two parts

$$
\varphi_{n,m}=\sum_{k=n}^{m-1}\alpha^{(0)}_k+\sum_{k=n}^{m-1}\Delta\alpha_k. \qquad (29)
$$

Here the angles $\alpha^{(0)}_k\equiv\varphi^{(0)}_{k,k+1}$ may be equal to 0 or π and specify the corresponding planar structure, while the angles $\Delta\alpha_k\equiv\Delta\varphi_{k,k+1}$ are relatively small and hence $\sin(\Delta\alpha_k)\approx\Delta\alpha_k$.

In this way, we can linearize Eq. (27) with respect to $\Delta\alpha_i$:

$$
\sum_{j=1}^{t-1}c_{i,j}\Delta\alpha_j=q_i. \qquad (30)
$$

The right-hand side q_i is defined as

$$
q_i=-2\frac{\chi c_{\rm p}c_{\rm f}}{B}\sum_{n=1}^{i}\sum_{m=i+1}^{t}f^{(1)}_{m-n+1}\cos\varphi^0_{n,m}, \qquad (31)
$$

which is Eq. (68) of Ref. [36]. The left-hand side $c_{i,j}$ is a $(t-1)$-dimensional matrix defined as for the lower off-diagonal elements ($i>j$, where $j=1,2,\ldots,t-2$ and $i=j+1,j+2,\ldots,t-1$)

$$
\begin{aligned}
c^{(\rm lower)}_{i,j}&=\frac{\chi c_{\rm p}c_{\rm f}}{B}\sum_{n=1}^{j}\sum_{m=i+1}^{t}\left(\frac{c_{\rm p}}{c_{\rm f}}f_{m-n+1}+\frac{c_{\rm f}}{c_{\rm p}}f^{(2)}_{m-n+1}\right)\cos\varphi^0_{n,m}\\
&\quad+2+\tilde{T}\cos\alpha^0_t\pm\tilde{E}\left(1-S\frac{\delta_{j,1}}{2}\right)\sum_{n=i+1}^{t}\cos\varphi^0_{1,n}, \qquad (32)
\end{aligned}
$$

for the diagonal elements ($i=j$, where $i=j=1,2,\ldots,t-1$)

$$
\begin{aligned}
c^{(\rm diagonal)}_{i,j}&=\frac{\chi c_{\rm p}c_{\rm f}}{B}\sum_{n=1}^{i}\sum_{m=i+1}^{t}\left(\frac{c_{\rm p}}{c_{\rm f}}f_{m-n+1}+\frac{c_{\rm f}}{c_{\rm p}}f^{(2)}_{m-n+1}\right)\\
&\quad\times\cos\varphi^0_{n,m}+4+\tilde{T}\left(\cos\alpha^0_i+\cos\alpha^0_t\right)\\
&\quad\pm\tilde{E}\left(1-S\frac{\delta_{i,1}}{2}\right)\left(1-S\frac{\delta_{j,1}}{2}\right)\\
&\quad\times\left(S\delta_{i,1}\delta_{j,1}+\sum_{n=i+1}^{t}\cos\varphi^{(0)}_{1,n}\right), \qquad (33)
\end{aligned}
$$

and for the upper off-diagonal elements ($i<j$, where $i=1,2,\ldots,t-2$ and $j=i+1,i+2,\ldots,t-1$)

$$
\begin{aligned}
c^{(\rm upper)}_{i,j}&=\frac{\chi c_{\rm p}c_{\rm f}}{B}\sum_{n=1}^{i}\sum_{m=j+1}^{t}\left(\frac{c_{\rm p}}{c_{\rm f}}f_{m-n+1}+\frac{c_{\rm f}}{c_{\rm p}}f^{(2)}_{m-n+1}\right)\cos\varphi^0_{n,m}\\
&\quad+2+\tilde{T}\cos\alpha^0_t\pm\tilde{E}\left(1-S\frac{\delta_{i,1}}{2}\right)\sum_{n=j+1}^{t}\cos\varphi^0_{1,n}, \qquad (34)
\end{aligned}
$$

where the plus and minus signs before $\tilde{E}$ represent cases (i) and (iii) and cases (ii) and (vi), respectively. The last terms containing $\tilde{E}$ in Eqs. (32)–(34) show the effect of an applied electric field, which result from the last term of Eq. (27); the other terms independent of $\tilde{E}$ have already been given in Eq. (69) of Ref. [36], although there exist some typographical errors in the original publication [36,51].

B. Numerical calculations

Now let us consider what superlattice structures are stabilized to become field-induced subphases on the higher field side of the three-layer $q_E=1/3$ subphase, particularly in the temperature region where the ferrielectric $q_T=1/3$ subphase stably exists at zero electric field $\tilde{E}=0$. Given the tilting sense R or L in a t-layer unit cell by assigning 0 or π for $\alpha^{(0)}_k\equiv\varphi^{(0)}_{k,k+1}$ in Eq. (29), we can use Eqs. (30)–(34) to uniquely determine the corresponding small deviation angles $\Delta\alpha_k\equiv\Delta\varphi_{k,k+1}$ that minimize the dimensionless free energy of Eq. (17). After checking all the possible sequences of $\alpha^{(0)}_k$, we can expect to obtain an optimal field-induced superlattice structure with the t-layer unit cell. Then, by comparing the free energies of the optimal structures with different-size unit cells with one another, we can determine the field-induced subphase that has the globally minimal free energy at a given applied electric field $\tilde{E}$ for a particular choice of the other four model parameters.

Taking all the possible structures into account is an orthodox way to determine the field-induced subphases that have the global minimal free energy. Pursuing simply this way is, however, obstructed by the large number of structures to be examined. The field-induced subphase observed by microbeam RXRS has an unexpected exceptional unit cell containing as many as 15 smectic layers, although the planar structure could not be successfully determined because the counting statistics was insufficient [33]. We need to check

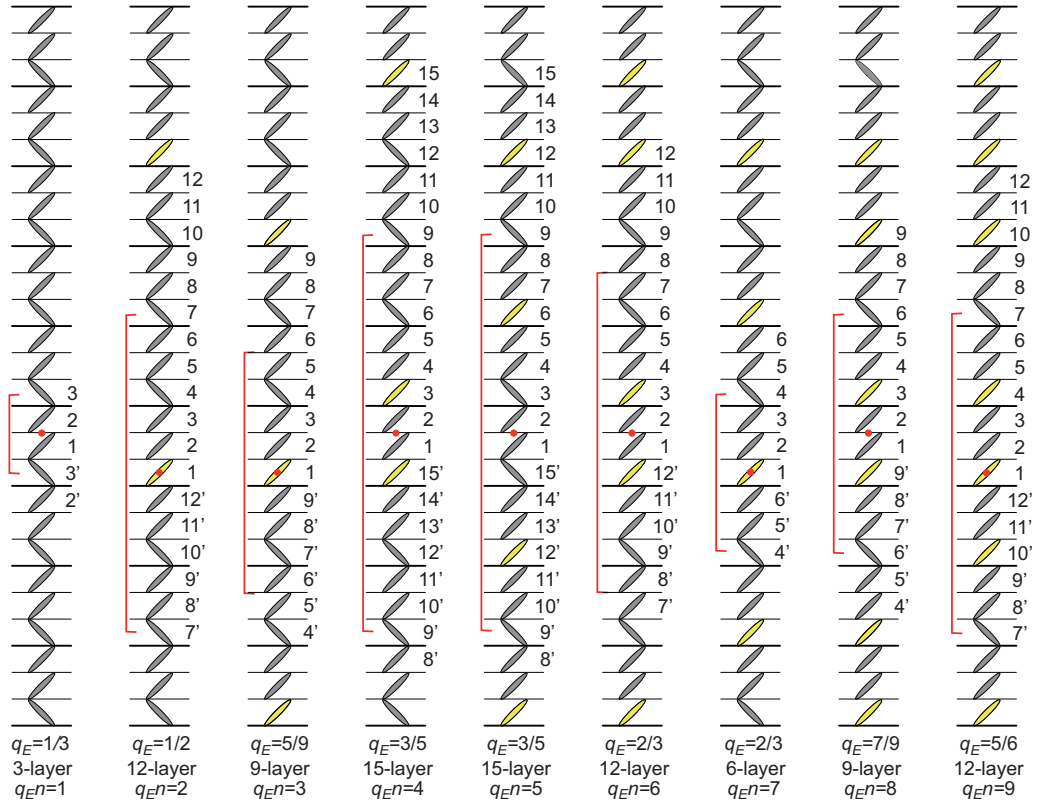

FIG. 2. Nine composite planar superlattice structures used in the free-energy calculation. We only need to calculate the free energy given in Eq. (17) using $\alpha_k^{(0)}$ in Eq. (29) for these nine, if we assume that any field-induced subphase in the temperature region of $q_T = 1/3$ consists of an orderly array of the 3-layer ferrielectric and ferroelectric blocks and that the largest unit cells are of 15-layer periodicity (5 blocks) with simple q_E in lower terms up to 7/9; notice that we have disregarded q_E in terms higher than 7/9 (either in numerator or denominator), i.e., 7/15, 11/15, and 13/15. Hereafter we designate these nine as $q_E n = 1, \ldots, 9$.

the free energy for field-induced superlattice structures with unit cells consisting of up to 15 smectic layers. The actual number of structures becomes much less than 2^{15}, because of the periodic boundary conditions and other equivalence properties, but is still more than 1000.

Instead of performing such comprehensive calculations, therefore, here we choose a more intuitive way on the basis of recent experimental findings by microbeam RXRS about the planar structure of the field-induced subphase with a 12-layer unit cell of $q_E = 2/3$. The unit cell can be regarded as a much simpler array of four building blocks, two ferrielectric and two ferroelectric. Each block would be originally the ferrielectric three-layer unit cell of the subphase $q_T = 1/3$ stabilized by the LRILIs, with two consecutive blocks modified to become ferroelectric by an applied electric field. There are three ways to choose the ferrielectric three-layer unit cell of $q_T = 1/3$. In any case, the unit cell contains only one unfavorable L layer, which the applied electric field may change into the favorable R layer, and the resulting unit cell becomes the unique ferroelectric block; hence the choice of the three-layer unit cell of $q_T = 1/3$ is not essential.

It is not impertinent to generalize the conclusion about the characteristic composite structure of the 12-layer $q_E = 2/3$ subphase. Let us consider that any field-induced subphase in the temperature region of $q_T = 1/3$ consists of an orderly array of the ferrielectric and ferroelectric blocks and that the relative ratio of the ferroelectric block becomes larger with increasing applied electric field. We need to consider five different sizes of the composite superlattice structures: The single-block (three-layer) structure has $q_E = 1/3$ and is basically the temperature-induced $q_T = 1/3$ subphase. The two-block (six-layer) structure has $q_E = 2/3$. There exist two three-block (nine-layer) structures that have $q_E = 5/9$ and 7/9, respectively. Similarly there are three four-block (12-layer) structures that have $q_E = 1/2$, 2/3, and 5/6, respectively. In the case of five-block (15-layer) structures, $q_E = 7/15$, 2/3, 11/15, and 13/15, which are not fractions in lower terms, except for $q_E = 2/3$. We have a disregard for these fractions in higher terms such as 7/15, 11/15, and 13/15 by simply assuming that unit cells with q_E's in lower terms must be observed easily. This way of simplification extremely reduces the number of planar superlattice structures to be examined when we search for a field-induced subphase. We only need to calculate the free energy given in Eq. (17) using $\alpha_k^{(0)}$ in Eq. (29) for the planar superlattice structures shown in Fig. 2 as well as for the Sm-C^* phase. Hereafter we designate these nine as $q_E n = 1, \ldots, 9$.

Actual calculations were performed for parameter values used in the classical paper [36,51], $\chi c_p c_f / B = -0.12$ and $c_f/c_p = -1.0$. Thus we reproduced their g-$\tilde{T}$ phase diagram and chose nine points for studying the electric-field effect as shown in Fig. 3. Table I illustrates calculated dimensionless

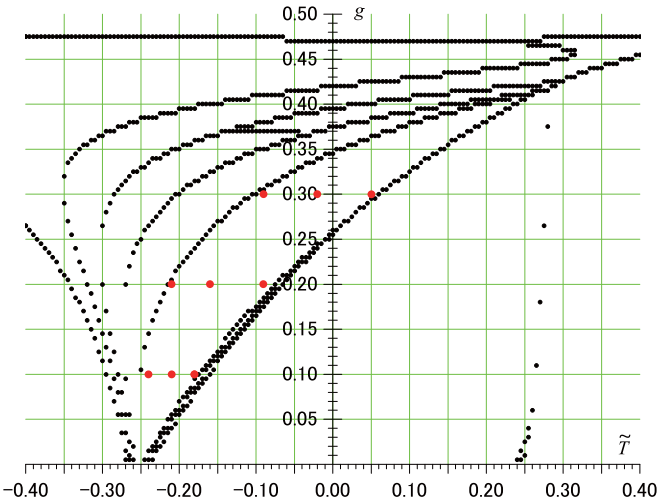

FIG. 3. Reproduced g-$\tilde{T}$ phase diagram with parameter values of $\chi c_p c_f/B = -0.12$ and $c_f/c_p = -1.0$ [36,51], and nine chosen points in red for studying the electric field effect: $\tilde{T} = -0.24$, -0.21, and -0.18 at $g = 0.1$; $\tilde{T} = -0.21$, -0.16, and -0.09 at $g = 0.2$; and $\tilde{T} = -0.09$, -0.02, and 0.05 at $g = 0.3$.

free energies for $g = 0.1$ and $\tilde{T} = -0.18$; similar results are obtained for the other g and $\tilde{T}$ values investigated. We begin with the limits of our analysis. Apparently, the direct field-induced transition occurs from $q_E n = 1$ to Sm-C^* and no sequential transitions among field-induced subphases are observed. This must be caused by the fact that the free energy of the actual Sm-C^* phase is not appropriately given by Eq. (19). All the subphases are not planar and have the microscopic short-pitch highly distorted helical structures, whereas the Sm-C^* phase is considered to be perfectly planar. Since the frustration actually occurs among the Sm-C^*_A, Sm-C^*, and Sm-A phases [8,27], the discrete flexoelectric effect produces the helical structure even in the Sm-C^* phase. The free energy of the Sm-C^* phase calculated by Eq. (19) must be lower than that of the actual field-induced unwound Sm-C^* phase and hence the direct field-induced transition from $q_E n = 1$ to Sm-C^* is always observed as illustrated in Table I. A more elaborate treatment should be made by taking into account the three-phase frustration among the Sm-C^*_A, Sm-C^*, and Sm-A phases as well as the temperature-dependent tilt angle θ. The direct field-induced transition from $q_E n = 1$ to $q_E n = 9$, the structure of which is quite similar to Sm-C^*, is also observed and invades the stability range of the other subphases that may participate in the sequential field-induced transitions. We have, therefore, a disregard for $q_E n = 9$ ($q_E = 5/6$) as well as Sm-C^* in the following.

Among the remaining eight field-induced superlattice structures $q_E n = 1, \ldots, 8$, the most stable $q_E n = 1$ is basically the temperature-induced $q_T = 1/3$ subphase at $\tilde{E} = 0$; it exists in a wide field range up to $\tilde{E} = 0.676$ and then makes the field-induced transition to $q_E n = 4$ at $\tilde{E} = 0.677$. The field-induced transition from $q_E n = 4$ to $q_E n = 6$ is observed at $\tilde{E} = 0.681$. The $q_E n = 6$ field-induced subphase has the 12-layer unit cell of $q_E = 2/3$ and exists as the second stable field-induced subphase for all the g values and temperatures investigated. The third stable field-induced subphase may be $q_E n = 4$ with the 15-layer unit cell of $q_E = 3/5$ in all the temperatures investigated for $g = 0.1$ and 0.2. Its stability range of $\tilde{E}$ is narrower in $g = 0.2$ than in 0.1; it is not stabilized for $g = 0.3$. Another field-induced transition from $q_E n = 6$ to $q_E n = 8$ may occur at 0.684. The $q_E n = 8$ field-induced subphase has the nine-layer unit cell of $q_E = 7/9$. Since

TABLE I. Calculated dimensionless free-energy densities $\tilde{F}_t$ for nine possible superlattice structures shown in Fig. 2 as well as Sm-C^* at $\tilde{T} = -0.18$ for $g = 0.1$. Aside from $q_E n = 9$ and Sm-C^*, $q_E n = 1$ has the smallest $\tilde{F}_t$ up to $\tilde{E} = 0.676$, but first $q_E n = 4$, second $q_E n = 6$, and then $q_E n = 8$ stabilize at $\tilde{E} = 0.677$, 0.681, and 0.684, respectively, as indicated by the corresponding $\tilde{F}_t$'s shown in boldface. Notice, however, that the direct transition from $q_E n = 1$ to $q_E n = 9$ always occurs when it is included. For details, see the text.

$\tilde{E}$	$q_E n = 1$ $q_E = 1/3$ 3-layer	$q_E n = 2$ $q_E = 1/2$ 12-layer	$q_E n = 3$ $q_E = 5/9$ 9-layer	$q_E n = 4$ $q_E = 3/5$ 15-layer	$q_E n = 5$ $q_E = 3/5$ 15-layer	$q_E n = 6$ $q_E = 2/3$ 12-layer	$q_E n = 7$ $q_E = 2/3$ 6-layer	$q_E n = 8$ $q_E = 7/9$ 9-layer	$q_E n = 9$ $q_E = 5/6$ 12-layer	Sm-C* $q_E = 1$ 1-layer
0	**− 1.31933**	− 1.20682	− 1.16855	− 1.14093	− 1.13772	− 1.09517	− 1.09117	− 1.01818	− 0.98139.	− 0.87
0.1	− 1.35237	− 1.25617	− 1.22349	− 1.19996	− 1.19710	− 1.16104	− 1.15732	− 1.09545	− 1.06423	− 0.97
0.2	− 1.38542	− 1.30561	− 1.27851	− 1.25923	− 1.25655	− 1.22706	− 1.22351	− 1.17279	− 1.14718	− 1.07
0.3	− 1.41848	− 1.35511	− 1.33356	− 1.31864	− 1.31607	− 1.29320	− 1.28974	− 1.25019	− 1.23020	− 1.17
0.4	− 1.45155	− 1.40466	− 1.38866	− 1.37815	− 1.37563	− 1.35941	− 1.35601	− 1.32763	− 1.31326	− 1.27
0.5	− 1.48463	− 1.45425	− 1.44381	− 1.43773	− 1.43523	− 1.42568	− 1.42231	− 1.40511	− 1.39636	− 1.37
0.6	− 1.51771	− 1.50387	− 1.49898	− 1.49736	− 1.49486	− 1.49200	− 1.48864	− 1.48262	− 1.47948	− 1.47
0.676	**− 1.54286**	− 1.54161	− 1.54094	− 1.54271	− 1.54020	− 1.54243	− 1.53906	− 1.54154	− 1.54267	− 1.546
0.677	− 1.54319	− 1.54210	− 1.54149	**− 1.54330**	− 1.54080	− 1.54309	− 1.53973	− 1.54232	− 1.54350	− 1.547
0.680	− 1.54419	− 1.54359	− 1.54315	**− 1.54509**	− 1.54259	− 1.54508	− 1.54172	− 1.54464	− 1.54600	− 1.550
0.681	− 1.54452	− 1.54409	− 1.54370	− 1.54569	− 1.54318	**− 1.54575**	− 1.54238	− 1.54542	− 1.54683	− 1.551
0.683	− 1.54518	− 1.54508	− 1.54480	− 1.54688	− 1.54438	**− 1.54708**	− 1.54371	− 1.54697	− 1.54849	− 1.553
0.684	− 1.54551	− 1.54558	− 1.55360	− 1.54748	− 1.54497	− 1.54774	− 1.54437	**− 1.54775**	− 1.54932	− 1.554
0.7	− 1.55081	− 1.55353	− 1.55419	− 1.55703	− 1.55452	− 1.55836	− 1.55499	− 1.56015	− 1.56263	− 1.57
0.8	− 1.58391	− 1.60321	− 1.60942	− 1.61674	− 1.61421	− 1.62474	− 1.62136	− 1.63771	− 1.64579	− 1.67
0.9	− 1.61702	− 1.65291	− 1.66467	− 1.67647	− 1.67391	− 1.69115	− 1.68775	− 1.71528	− 1.72897	− 1.77
1	− 1.65013	− 1.70263	− 1.71995	− 1.73622	− 1.73364	− 1.75758	− 1.75416	− 1.79287	− 1.81216	− 1.87

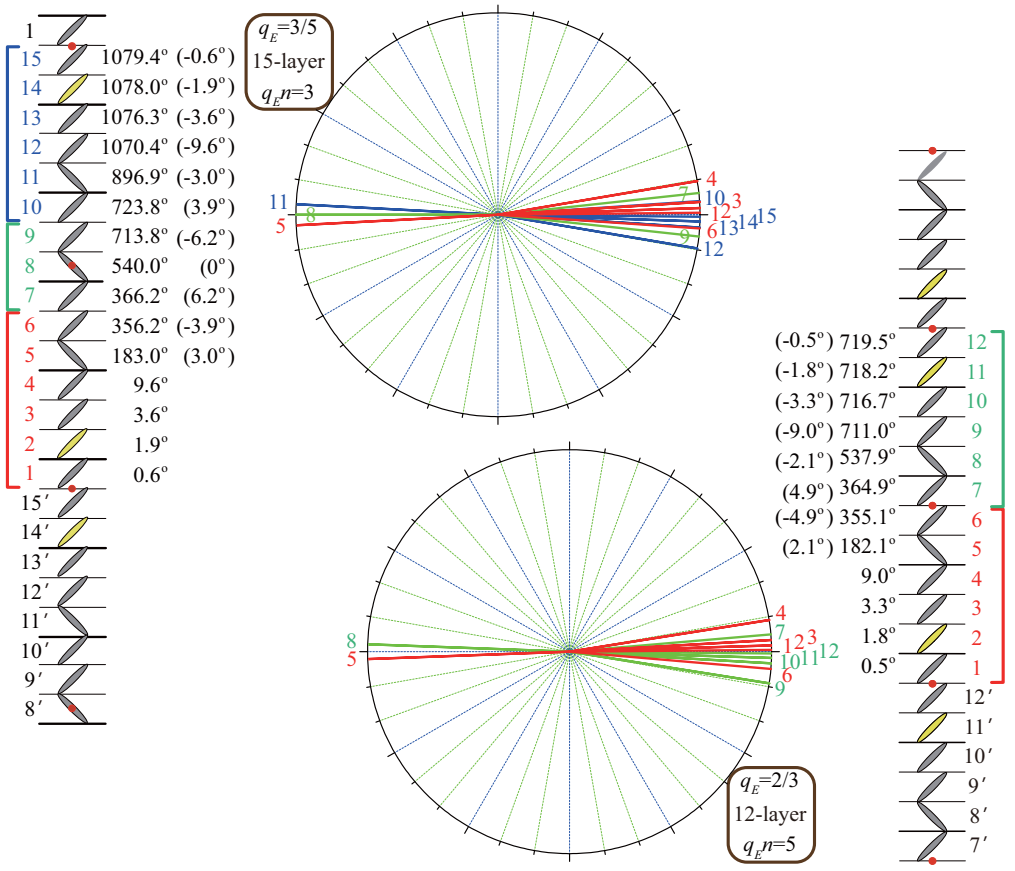

FIG. 4. Calculated φ_i for $q_E n = 4$ at $\tilde{E} = 0.573$ and for $q_E n = 6$ at $\tilde{E} = 0.574$. Other parameters are $g = 0.2, \tilde{T} = -0.09$, $\chi c_p c_f / B = -0.12$, and $c_p/c_f = -1.0$. The relevant dimensionless free energies are -1.5113 for $q_E n = 1$ at $\tilde{E} = 0.572$, -1.51166 for $q_E n = 4$ at $\tilde{E} = 0.573$, and -1.51228 for $q_E n = 6$ at $\tilde{E} = 0.574$. The electric field is applied along the y axis and it is assumed that $c_p > 0$ and hence that the spontaneous polarization is positive and the microscopic short-pitch distorted helix is right handed. The tilt directions in different layers are symmetrical with respect to the middle of the period indicated by closed red circles; this property defines the chirality of these subphases.

$q_E n = 8$ is rather close to the Sm-C^* phase and its q_E is hardly regarded as a fraction in lower terms, it may not exist as a single independent stable subphase; it may overlap with other similar field-induced subphases. The remaining $q_E n = 2, 3, 5$, and 7 are not stabilized at all and hence do not exist as the field-induced subphases.

Figure 4 shows the microscopic short-pitch helical structures of the $q_E n = 4$ and 6 subphases with the 15-layer and 12-layer unit cells, respectively. The calculations were made in the linearized approximation explained in Sec. IV B. The $q_E n = 4$ helix makes three rotations in the 15-layer unit cell, whereas the $q_E n = 6$ helix makes two rotations in the 12-layer unit cell. The director tilting directions of all smectic layers are arranged symmetrically with respect to the z-x plane. As we expected, the deviation from the planar structures is small in both subphases. At the same time, we notice that the deviation is slightly larger in the $q_E n = 4$ helix than in the $q_E n = 6$ helix, when we compare both helices carefully. As a measure of the deviation $\mathcal{D}$, we calculated

$$\mathcal{D} = \frac{1}{t} \sum_{i=1}^{t} |\sin \phi_i| \tag{35}$$

and actually obtained $\mathcal{D} = 0.067$ and 0.063 for the $q_E n = 4$ and 6 helices, respectively.

V. DISCUSSION

The calculated results are entirely consistent with the recent microbeam RXRS data [33]. The experiments were performed using a slightly unusual compound that has chiral centers in both terminal chains and a bromine atom in its central core part; the chemical structure is given in Fig. 5. The phase sequence is, however, quite ordinary [52]: Sm-C_A^*–1/3–1/2–Sm-C^*–Sm-C_α^*–Sm-A–Iso. The prototypal subphases $q_T = 1/3$ and 1/2 emerge between the main phases Sm-C_A^* and Sm-C^*; hence it is legitimate to consider that the subphases are produced by the frustration between antiferroelectric Sm-C_A^* and ferroelectric Sm-C^* phases and to use the approximation that the tilt angle is relatively large, spatially uniform, and temperature independent. As explained in Sec. II, in fact, we have calculated the free energy based on this approximation

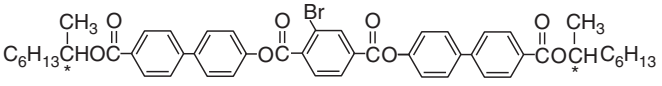

FIG. 5. The compound Iida *et al.* used in the recent microbeam RXRS experiments [33]. The two chiral centers are (S,S). They noticed the emergence of the field-induced subphases that have unbelievably large 12- and 15-layer unit cells.

relying on the LRILIs introduced by Emelyanenko and Osipov [36], disregarding that the actual frustration occurs among the three main phases Sm-C_A^*, Sm-C^*, and Sm-A [8]. Furthermore, the calculations have been performed for field-induced superlattice structures that may emerge on the higher field side of the three-layer $q_E = 1/3$ subphase. The microbeam RXRS data were taken in three different temperature regions of Sm-C_A^* (140 °C), $q_T = 1/3$ (144 °C), and $q_T = 1/2$ (145.1 °C and 146 °C); all of them show nearly the same tendency that field-induced superlattice subphases may emerge on the higher field side of the three-layer $q_E = 1/3$ subphase, except for the data at 146 °C; hence we choose the most elaborate data at 140 °C shown in Fig. 7 of Ref. [33] and compare them with the calculated results in the following.

The experimental results indicate that the three-layer periodicity prevails in a wide electric field range and that not only the 12-layer but also the 15-layer periodicity is inseparably observed as a spotty pattern in a narrow electric field region, above which the spotty pattern changes into a diffuse streak pattern just before the field-induced transition to the Sm-C^* phase occurs. The three-layer periodicity must basically result from the $q_E n = 1$ field-induced superlattice structure, i.e., the three-layer unit cell of the temperature-induced $q_T = 1/3$ subphase together with its behavior in an applied electric field described in Sec. III. As exemplified in Table I, the stability range of $q_E n = 1$ is pretty wide. It stably exists up to $\tilde{E} = 0.676$ and then three field-induced transitions stabilize $q_E n = 4$ at $\tilde{E} = 0.677$, $q_E n = 6$ at $\tilde{E} = 0.681$, and $q_E n = 8$ at $\tilde{E} = 0.684$ sequentially. The field-induced subphases $q_E n = 4$ and 6 have a 15-layer unit cell of $q_E = 3/5$ and a 12-layer unit cell of $q_E = 2/3$, respectively; their stability ranges are very narrow. As explained in Sec. IV B, $q_E n = 8$ is rather close to Sm-C^* and may not be observed as a single independent subphase due to overlapping with other subphases.

In this way, the observed 15-layer and 12-layer periodic spotty patterns naturally correlate with the field-induced subphases $q_E n = 4$ and 6 in Table I, respectively; the observed diffuse streak pattern may result from some overlapped field-induced subphases including $q_E n = 8$, which have large unit cells and complex q_E's in higher terms and become inevitably disordered by a number of factors. The experimentally confirmed fact that the nine-layer and six-layer periodicities were not observed correlates with the calculated results that $q_E n = 3$ and 7 are not stabilized in Table I. Experimentally, the microbeam RXRS could not confirm the existence of $q_E n = 2$ consisting of four three-layer blocks, three ferrielectric and one ferroelectric, which produce almost the same satellite peak intensity distribution (strong m/3-order satellites) as the original three-layer $q_E = 1/3$ phase, $q_E n = 1$. The calculated results illustrated in Table I show that $q_E n = 2$, the 12-layer field-induced superlattice structure of $q_E = 1/2$, does not stably exist as a field-induced subphase.

Now let us investigate the satellite peak intensity distribution patterns further. By using the Osipov-Gorkunov formula [53] to obtain RXRS intensities for all possible planar structures with 12-layer periodicity, as illustrated in Fig. 8 of Ref. [33], it was concluded that only two planar structures with $q_E = 2/3$ and $1/6$ were consistent with the experimentally observed intensity distribution. Since the 12-layer structure was produced by the field-induced transition from the three-layer structure with $q_E = 1/3$ in all the temperatures investigated, except for 146 °C, the 12-layer structure with $q_E = 1/6$ was considered improbable [33]. Notice that the remaining 12-layer structure with $q_E = 2/3$ is exactly the same as the most stable calculated $q_E n = 6$ with the 12-layer unit cell shown in Fig. 2.

Regarding the 15-layer unit cell, the RXRS data given in Fig. 7 of Ref. [33] clearly indicate the emergence of a field-induced subphase with a 15-layer unit cell but could not determine its planar structure because the signal intensity is weak. However, the RXRS data are consistent with the calculated result that an applied electric field may stabilize $q_E n = 4$ but not $q_E n = 5$. The Osipov-Gorkunov formula [53] indicates that the RXRS intensities of 4/15 and 6/15 are about 1/4 of the intensity of 5/15 in $q_E n = 4$, whereas the intensities are about 1/24 in $q_E n = 5$. As clearly shown in Fig. 7 of Ref. [33], the RXRS intensities of 4/15 and 6/15 are closer to 1/4 and hence we can conclude that the applied electric field stabilizes $q_E n = 4$.

Figure 4 shows that the deviation from the planar structure in the $q_E n = 6$ subphase is slightly smaller than that in the $q_E n = 4$ subphase and in fact the measure of deviation defined by Eq. (35) is smaller in the $q_E n = 6$ subphase than that in the $q_E n = 4$ subphase. Suppose we observe the electric-field-induced birefringence (EFIB) at 144 °C by increasing the applied electric field: The EFIB first rises sharply due to the unwinding of the macroscopic long-pitch helical structure. When the field-induced $q_E n = 1$ subphase prevails, EFIB stays almost constant in a wide applied electric-field range. Just before the field-induced transition to the unwound Sm-C^* phase occurs, EFIB once decreases slightly and then increases again when $q_E n = 4$ and 6 emerge consecutively in a narrow electric-field range. In the electric-field–temperature E-T phase diagram, characteristic sigmoid-shaped birefringence contours are expected to be observed in the neighborhood of subsequent decreasing and increasing. Although in different materials Sandhya *et al.* actually observed the sigmoid-shaped contours in the MHPOCBC-MHPOOCBC binary mixture system as given in Figs. 2(i)–2(k) of Ref. [4]. They referred to the emergence of several field-induced subphases, but did not suggest such large unit cells of 12- and 15-layer periodicity shown in Fig. 4. Their microscopic short-pitch distorted helical structures have not yet been verified experimentally by using polarized RXRS experiments.

In this way the prototypal quasimolecular model based on the effective LRILIs proposed by Emelyanenko and Osipov [36] can explain the sequential emergence of the field-induced subphases with exceptionally large unit cells consisting of 12 and 15 smectic layers. In the $q_T = 1/3$ temperature region, the field-induced subphases may consist of several blocks, each of which would be originally the ferrielectric three-layer unit cell of the subphase $q_T = 1/3$ stabilized by the LRILIs but some of which are modified to become ferroelectric by an applied electric field; they are appropriately specified by their q_E numbers given in Eq. (2), which may increase monotonically from 1/3 to 1 with increasing applied electric field. It also predicts the highly distorted microscopic short-pitch helical director arrangements in the field-induced subphases and that

the deviation from the planar structure in $q_E n = 4$ is larger than that in $q_E n = 6$; EFIB may decrease slightly and then increase again as actually observed, although in different materials [4]. A weak point of this simplest way of treating lies in the fact that the Sm-C^* phase is considered to be perfectly planar in the prototypal quasimolecular model. Actually, however, the discrete flexoelectric effect produces the helical structure even in the Sm-C^* phase, since the frustration occurs among the Sm-C^*_A, Sm-C^*, and Sm-A phases. A more elaborate treatment should be made by taking into account the three-phase frustration as well as the temperature-dependent tilt angle θ as actually made at $\tilde{E} = 0$ preliminarily [7–9,27]. This treatment may also explain the characteristic evolution of the subphase emergence observed in several binary mixture systems [2,4].

ACKNOWLEDGMENTS

This work was partly supported by an Ireland-Japan International Strategic Cooperation Award and 13/US/I2866 Science Foundation Ireland grant as part of the USA-Ireland Research and Development Partnership program jointly administered with the United States National Science Foundation under Grant No. NSF-DMR-1410649. The authors thank Prof. M. A. Osipov of University of Strathclyde, Glasgow, Scotland for discussions.

[1] T. Isozaki, T. Fujikawa, H. Takezoe, A. Fukuda, T. Hagiwara, Y. Suzuki, and I. Kawamura, Phys. Rev. B **48**, 13439 (1993).
[2] A. Fukuda, Y. Takanishi, T. Isozaki, K. Ishikawa, and H. Takezoe, J. Mater. Chem. **4**, 997 (1994).
[3] A. D. L. Chandani, N. M. Shtykov, V. P. Panov, A. V. Emelyanenko, A. Fukuda, and J. K. Vij, Phys. Rev. E **72**, 041705 (2005).
[4] K. L. Sandhya, J. K. Vij, A. Fukuda, and A. V. Emelyanenko, Liq. Cryst. **36**, 1101 (2009).
[5] J. Prost and R. Bruinsma, Ferroelectrics **148**, 25 (1993).
[6] R. Bruinsma and J. Prost, J. Phys. (France) II **4**, 1209 (1994).
[7] M. A. Osipov and A. Fukuda, Phys. Rev. E **62**, 3724 (2000).
[8] N. M. Shtykov, A. D. L. Chandani, A. V. Emelyanenko, A. Fukuda, and J. K. Vij, Phys. Rev. E **71**, 021711 (2005).
[9] A. V. Emelyanenko and K. Ishikawa, Soft Matter **9**, 3497 (2013).
[10] C. C. Huang, S. Wang, L. Pan, Z. Q. Liu, B. K. McCoy, Y. Sasaki, K. Ema, P. Barois, and R. Pindak, Liq. Cryst. Rev. **3**, 58 (2015).
[11] P. Mach, R. Pindak, A.-M. Levelut, P. Barois, H. T. Nguyen, C. C. Huang, and L. Furenlid, Phys. Rev. Lett. **81**, 1015 (1998).
[12] P. Mach, R. Pindak, A.-M. Levelut, P. Barois, H. T. Nguyen, H. Baltes, M. Hird, K. Toyne, A. Seed, J. W. Goodby, C. C. Huang, and L. Furenlid, Phys. Rev. E **60**, 6793 (1999).
[13] A.-M. Levelut and B. Pansu, Phys. Rev. E **60**, 6803 (1999).
[14] T. Akizuki, K. Miyachi, Y. Takanishi, K. Ishikawa, H. Takezoe, and A. Fukuda, Jpn. J. Appl. Phys. **38**, 4832 (1999).
[15] P. M. Johnson, D. A. Olson, S. Pankratz, T. Nguyen, J. Goodby, M. Hird, and C. C. Huang, Phys. Rev. Lett. **84**, 4870 (2000).
[16] A. Cady, J. A. Pitney, R. Pindak, L. S. Matkin, S. J. Watson, H. F. Gleeson, P. Cluzeau, P. Barois, A.-M. Levelut, W. Caliebe, J. W. Goodby, M. Hird, and C. C. Huang, Phys. Rev. E **64**, 050702(R) (2001).
[17] I. Musevic and M. Skarabot, Phys. Rev. E **64**, 051706 (2001).
[18] N. M. Shtykov, J. K. Vij, and H. T. Nguyen, Phys. Rev. E **63**, 051708 (2001).
[19] N. M. Shtykov, J. K. Vij, R. A. Lewis, M. Hird, and J. W. Goodby, Liq. Cryst. **28**, 1699 (2001).
[20] N. W. Roberts, S. Jaradat, L. S. Hirst, M. S. Thurlow, Y. Wang, S. T. Wang, Z. Q. Liu, C. C. Huang, J. Bai, R. Pindak, and H. F. Gleeson, Europhys. Lett. **72**, 976 (2005).
[21] P. Fernandes, P. Barois, E. Grelet, F. Nallet, J. W. Goodby, M. Hird, and J.-S. Micha, Eur. Phys. J. E **20**, 81 (2006).
[22] P. D. Brimicombe, N. W. Roberts, S. Jaradat, C. Southern, S.-T. Wang, C.-C. Huang, E. DiMasi, R. Pindak, and H. F. Gleeson, Eur. Phys. J. E **23**, 281 (2007).
[23] S. Wang, L. D. Pan, R. Pindak, Z. Q. Liu, H. T. Nguyen, and C. C. Huang, Phys. Rev. Lett. **104**, 027801 (2010).
[24] V. P. Panov, N. M. Shtykov, A. Fukuda, J. K. Vij, Y. Suzuki, R. A. Lewis, M. Hird, and J. W. Goodby, Phys. Rev. E **69**, 060701(R) (2004).
[25] A. D. L. Chandani, A. Fukuda, S. Kumar, and J. K. Vij, Liq. Cryst. **38**, 663 (2011).
[26] Y. Takanishi, I. Nishiyama, J. Yamamoto, Y. Ohtsuka, and A. Iida, Phys. Rev. E **87**, 050503(R) (2013).
[27] K. L. Sandhya, A. D. L. Chandani, A. Fukuda, S. Kumar, and J. K. Vij, Phys. Rev. E **87**, 062506 (2013).
[28] K. Hiraoka, Y. Takanishi, K. Skarp, H. Takezoe, and A. Fukuda, Jpn. J. Appl. Phys. **30**, L1819 (1991).
[29] T. Isozaki, T. Fujikawa, H. Takezoe, A. Fukuda, T. Hagiwara, Y. Suzuki, and I. Kawamura, Jpn. J. Appl. Phys. **31**, L1435 (1992).
[30] N. M. Shtykov, J. K. Vij, R. A. Lewis, M. Hird, and J. W. Goodby, Phys. Rev. E **62**, 2279 (2000).
[31] S. Jaradat, P. D. Brimicombe, C. Southern, S. D. Siemianowski, E. DiMasi, M. Osipov, R. Pindak, and H. F. Gleeson, Phys. Rev. E **77**, 010701(R) (2008).
[32] K. L. Sandhya, A. Fukuda, and J. K. Vij, Mol. Cryst. Liq. Cryst. **511**, 36/[1506] (2009).
[33] A. Iida, I. Nishiyama, and Y. Takanishi, Phys. Rev. E **89**, 032503 (2014).
[34] P. V. Dolganov, V. M. Zhilin, V. K. Dolganov, and E. I. Kats, Phys. Rev. E **83**, 061705 (2011).
[35] P. V. Dolganov and E. I. Kats, Liq. Cryst. Rev. **1**, 127 (2013).
[36] A. V. Emelyanenko and M. A. Osipov, Phys. Rev. E **68**, 051703 (2003).
[37] A. V. Emelyanenko and M. A. Osipov, Ferroelectrics **309**, 13 (2004).
[38] T. Qian and P. L. Taylor, Phys. Rev. E **60**, 2978 (1999).
[39] L. A. Parry-Jones and S. J. Elston, Phys. Rev. E **63**, 050701(R) (2001).
[40] L. A. Parry-Jones and S. J. Elston, Appl. Phys. Lett. **79**, 2097 (2001).
[41] J.-K. Song, A. Fukuda, and J. K. Vij, Phys. Rev. Lett. **101**, 097801 (2008).
[42] J. K. Song, A. Fukuda, and J. K. Vij, Phys. Rev. E **78**, 041702 (2008).

[43] Y. Suzuki, G.-P. Chen, U. Manna, J. K. Vij, and A. Fukuda, Appl. Phys. Express **2**, 071403 (2009).
[44] P. V. Dolganov, V. M. Zhilin, V. K. Dolganov, and E. I. Kats, Phys. Rev. E **86**, 020701(R) (2012).
[45] A. V. Emelyanenko, Eur. Phys. J. E **28**, 441 (2009).
[46] A. V. Emelyanenko, Phys. Rev. E **82**, 031710 (2010).
[47] A. V. Emelyanenko, Ferroelectrics **495**, 129 (2016).
[48] M. Johno, K. Itoh, J. Lee, Y. Ouchi, H. Takezoe, A. Fukuda, and T. Kitazume, Jpn. J. Appl. Phys. **29**, L107 (1990).
[49] K. Hiraoka, H. Takezoe, and A. Fukuda, Ferroelectrics **147**, 13 (1993).
[50] J.-K. Song, A. Fukuda, and J. K. Vij, Appl. Phys. Lett. **93**, 142903 (2008).
[51] A. Fukuda, Mol. Cryst. Liq. Cryst. **610**, 1 (2015).
[52] Y. Takanishi, I. Nishiyama, J. Yamamoto, Y. Ohtsuka, and A. Iida, J. Mater. Chem. **21**, 4465 (2011).
[53] M. A. Osipov and M. V. Gorkunov, Liq. Cryst. **33**, 1133 (2006).